NeuroImage 56 (2011) 1251–1258

Contents lists available at ScienceDirect

NeuroImage

journal homepage: www.elsevier.com/locate/ynimg

Morphological and functional midbrain phenotypes in *Fibroblast Growth Factor 17* mutant mice detected by Mn-enhanced MRI

Xin Yu [a,1], Brian J. Nieman [a,2], Anamaria Sudarov [e], Kamila U. Szulc [a], Davood J. Abdollahian [a], Nitin Bhatia [d], Anil K. Lalwani [d], Alexandra L. Joyner [e], Daniel H. Turnbull [a,b,c,*]

[a] *Kimmel Center for Biology and Medicine at the Skirball Institute of Biomolecular Medicine, New York University School of Medicine, New York NY, USA*
[b] *Departments of Radiology, New York University School of Medicine, New York NY, USA*
[c] *Department of Pathology, New York University School of Medicine, New York NY, USA*
[d] *Department of Otolaryngology, New York University School of Medicine, New York NY, USA*
[e] *Developmental Biology Program, Sloan-Kettering Institute, New York NY, USA*

ARTICLE INFO

Article history:
Received 22 November 2010
Revised 14 February 2011
Accepted 17 February 2011
Available online 26 February 2011

Keywords:
MEMRI
DBM
IC
Activity mapping
Auditory
Tonotopic map

ABSTRACT

With increasing efforts to develop and utilize mouse models of a variety of neuro-developmental diseases, there is an urgent need for sensitive neuroimaging methods that enable *in vivo* analysis of subtle alterations in brain anatomy and function in mice. Previous studies have shown that the brains of *Fibroblast Growth Factor 17* null mutants (*Fgf17*$^{-/-}$) have anatomical abnormalities in the inferior colliculus (IC)—the auditory midbrain—and minor foliation defects in the cerebellum. In addition, changes in the expression domains of several cortical patterning genes were detected, without overt changes in forebrain morphology. Recently, it has also been reported that *Fgf17*$^{-/-}$ mutants have abnormal vocalization and social behaviors, phenotypes that could reflect molecular changes in the cortex and/or altered auditory processing / perception in these mice. We used manganese (Mn)-enhanced magnetic resonance imaging (MEMRI) to analyze the anatomical phenotype of *Fgf17*$^{-/-}$ mutants in more detail than achieved previously, detecting changes in IC, cerebellum, olfactory bulb, hypothalamus and frontal cortex. We also used MEMRI to characterize sound-evoked activity patterns, demonstrating a significant reduction of the active IC volume in *Fgf17*$^{-/-}$ mice. Furthermore, tone-specific (16- and 40-kHz) activity patterns in the IC of *Fgf17*$^{-/-}$ mice were observed to be largely overlapping, in contrast to the normal pattern, separated along the dorsal-ventral axis. These results demonstrate that *Fgf17* plays important roles in both the anatomical and functional development of the auditory midbrain, and show the utility of MEMRI for *in vivo* analyses of mutant mice with subtle brain defects.

Introduction

Several secreted proteins in the *Fibroblast Growth Factor* (*Fgf*) family are critical for neural patterning during embryogenesis. Among these, Fgf8 has been shown to be the main molecule responsible for "organizer" activity–the ability of a cell or tissue to send signals that instruct the fates of surrounding cells—during development of the mid-hindbrain (MHB) region (Crossley et al., 1996; Lee et al., 1997; Ye et al., 1998; Sato et al., 2001), and is also critical for normal forebrain development (Shimamura and Rubenstein, 1997; Meyers et al., 1998; Ye et al., 1998; Fukuchi-Shimogori and Grove, 2001; Garel et al., 2003; Storm et al., 2006). *Fgf17* expression overlaps with *Fgf8*, and also plays a role in the development of the MHB and cortex (Hoshikawa et al., 1998; Maruoka et al., 1998; Xu et al., 1999, 2000; Reifers et al., 2000; Liu et al., 2003; Fukuchi-Shimogori and Grove, 2003). While *Fgf8*$^{-/-}$ mice are embryonic lethal, *Fgf17*$^{-/-}$ mice are viable and fertile, having mild defects in the MHB, including (non-quantified) reduction of the inferior colliculus (IC), and small foliation changes in the cerebellum (Xu et al., 2000). *Fgf17*$^{-/-}$ mutants also show altered expression domains of genes that mark sub-regions of frontal cortex, without any obvious change in forebrain morphology (Cholfin and Rubenstein, 2007, 2008).

Interestingly, *Fgf17*$^{-/-}$ mice exhibit abnormal social behaviors, including decreased vocalization in pups and deficits in several adult behaviors involving social interactions, reminiscent of autism in humans (Scearce-Levie et al., 2008). It was suggested that these abnormal behaviors may result from altered forebrain function, based

Abbreviations: ABR, auditory brainstem recording; DBM, deformation based morphometry; Fgf17, fibroblast growth factor 17; IC, inferior colliculus; MRI, magnetic resonance imaging; MEMRI, manganese (Mn)-enhanced MRI.

* Corresponding author at: Skirball Institute of Biomolecular Medicine, New York University School of Medicine, 540 First Avenue, New York, NY 10016, USA. Fax: +1 212 263 8214.
E-mail address: Daniel.Turnbull@med.nyu.edu (D.H. Turnbull).
[1] Current address: Laboratory of Functional and Molecular Imaging, National Institute of Neurological Disorders and Stroke, Bethesda, MD, USA.
[2] Current address: Mouse Imaging Centre, Hospital for Sick Children and Toronto Centre for Phenogenomics, Toronto ON, Canada.

1053-8119/$ – see front matter © 2011 Elsevier Inc. All rights reserved.
doi:10.1016/j.neuroimage.2011.02.068

on evidence of reduced activation of the immediate early-gene *Fos* in *Fgf17*$^{-/-}$ frontal cortex after exploration of novel environments (Scearce-Levie et al., 2008). However, it is unclear whether altered auditory function, as a result of the known defects in the IC, the auditory midbrain, also contributes to the behavioral phenotypes in *Fgf17*$^{-/-}$ mice.

We hypothesized that whole brain anatomical MRI analysis would provide a more complete and quantitative characterization of the *Fgf17*$^{-/-}$ mouse morphological phenotype than previous qualitative studies based on histology. We also sought to investigate the possibility that *Fgf17*$^{-/-}$ mice have altered auditory function as a result of the reduction in IC. Previously, we have shown that MEMRI can be used to detect and analyze sound-evoked activity patterns in the mouse IC (Yu et al., 2005, 2007, 2008), based on the activity-dependent accumulation of paramagnetic Mn ions in neural cells *via* uptake through voltage-gated calcium channels (Lin and Koretsky, 1997). In addition to characterizing the normal mouse IC, we also demonstrated the utility of MEMRI to analyze altered IC activity patterns in mice exposed to atypical sound-rearing environments during auditory brain development (Yu et al., 2007). In the current study, we employed similar MEMRI-based functional analysis approaches to characterize differences in IC activity patterns, comparing *Fgf17*$^{-/-}$ mice and control littermates. Our findings of altered auditory function in *Fgf17*$^{-/-}$ mutants may help to explain at least some of the behavioral phenotypes that have been reported in these mice.

Materials and methods

Animals

All mice used in these studies were maintained under protocols approved by the Institutional Animal Care and Use Committee of New York University School of Medicine. *Fgf17* mutant mice were obtained from the Ornitz lab (Washington University), and *Fgf17*$^{+/-}$ x *Fgf17*$^{+/-}$ breeding pairs were mated to produce littermate *Fgf17*$^{+/+}$ wildtype (WT), *Fgf17*$^{+/-}$ heterozygous and *Fgf17*$^{-/-}$ homozygous mutants, while *Fgf17*$^{-/-}$×*Fgf17*$^{+/-}$ breeding pairs were mated to produce littermate *Fgf17*$^{+/-}$ and *Fgf17*$^{-/-}$ mice. Genotype analysis was performed *via* polymerase chain reaction from tail DNA, using primers CP3:TTGGCTTCTCTGGGACTCTACC; cre2:CCATGAGTGAACGAACCTGG to detect the mutant allele, and r1:GACAGCAGAGAATCAATAGCTGC; r2: GAAGTTTCTCCAGCGATGGG to detect wild type *Fgf17*, as described previously (Basson et al., 2008).

For MEMRI, WT, *Fgf17*$^{+/-}$, and *Fgf17*$^{-/-}$ mice were injected intraperitoneally (IP) with an aqueous solution of $MnCl_2$ (0.4 mmol/kg) one day before imaging (Yu et al., 2005, 2007). After injection, mice were placed in a controlled acoustic environment inside an acoustic isolation chamber (Mac-1, Industrial Acoustics) for 24-h. During this time, mice were maintained under normal living conditions, including a 12-h light / 12-h dark cycle and free access to food and water. Neither $MnCl_2$ administration, nor sound stimulation, induced any obvious abnormal behavior during the 24-h time period.

Auditory brainstem recordings

Auditory brainstem recordings (ABR) were measured using calibrated equipment and protocols, as described in detail by Willott (2006). Prior to ABR testing, mice were anesthetized with an intramuscular injection of a mixture of ketamine (50 mg/kg) and xylazine (95 mg/kg). ABR testing was performed in a double-walled acoustic chamber (Industrial Acoustics), using an isothermic heating pad (K20, Baxter) to maintain body temperature at 36–38 °C. Silver electrodes were inserted subcutaneously at the vertex of the skull, and just inferior to each ear (ispilateral = reference; contralateral = ground). The biological signal, between the vertex and reference electrodes, was amplified (DAM-50E, World Precision Instruments), bandpass filtered from 0.3 to 3 kHz, 90 dB/octave, (VBF8.04, Stewart Electronics), digitized at a 25-kHz sampling rate and recorded over a 10-ms window (System II, Tucker Davis Technologies). Response was measured to both click and pure tone (8-, 16-, 24- and 32-kHz) stimuli, decreasing the amplitude in 5-dB steps, from 95 to 5 dB peak sound pressure level (SPL). Threshold was determined as the level one step above that where no discernible ABR waveform was detected. Differences in the threshold data for the three genotypes were analyzed statistically with ANOVA (one-way). Note that 32-kHZ was the highest frequency that could be achieved reliably with the existing ABR recording system.

MRI data acquisition

MEMRI imaging was performed as described in detail previously (Yu et al., 2005, 2007). Briefly, T1-weighted brain images were acquired with a 3D gradient echo pulse sequence (echo time, TE = 4-ms; repetition time, TR = 50-ms; flip angle = 65°), resulting in a volumetric image set covering the entire brain, with isotropic spatial resolution of 100-μm in a total imaging time of 110 min per mouse. MRI was performed on a micro-imaging system (SMIS) consisting of a 7-Tesla horizontal magnet (Magnex Scientific) with actively shielded gradients (Magnex: 250-mT/m gradient strength; 200-μs rise time) and a 25-mm (inner diameter) quadrature Litzcage mouse head coil (Doty Scientific). All mice were imaged at 3 weeks of age (postnatal days 21–24, P21–24), where P0 denotes the day of birth.

Acoustic stimulation protocol

The acoustic environment and sound stimuli were described in detail previously (Yu et al., 2005, 2007). Sound stimulation in the current study consisted of calibrated broadband sound (1–59 kHz) and single tones (16- and 40-kHz) played through a speaker mounted inside the acoustic isolation chamber. The carrier frequencies were amplitude modulated at 4-Hz with a modulation range of 90%. For all experiments, the amplitude-modulated stimuli had peak amplitudes of 89 dB SPL, measured at the calibration point in the geometrical center of the cage, 10-cm above the cage bottom (Yu et al., 2007).

For tonotopic (pure tone) studies, mice were first imaged at P21, after injection of $MnCl_2$ (0.4-mmol/kg, IP) at P20 and 24 h of exposure to 40-kHz. The same mice were subsequently kept in a quiet environment for two days, and then injected IP with a second, smaller dose of $MnCl_2$ (0.2-mmol/kg, IP) at P23 for imaging at P24 after 24 h of exposure to 16-kHz. For comparison, a separate group of *Fgf17*$^{-/-}$ mice was imaged at P21, 24 h after injection of $MnCl_2$ (0.4-mmol/kg) and exposure to 16-kHz. The 16-kHz activity patterns at age P21 and P24 were compared to determine the effects of mouse age and the longitudinal experimental protocol on the MEMRI enhancement patterns and the resulting statistical maps.

Histology and immunohistochemistry

Mice were anesthetized *via* IP injection of a mixture of ketamine (100-mg/kg) and xylazine (10-mg/kg) in phosphate buffered saline (PBS) and perfused transcardially with PBS, followed by 4% paraformaldehyde. For frozen sections, the brains were removed quickly, post-fixed for 24-h in 4% paraformaldehyde at 4 °C, and cryoprotected in (4 °C) 15% and 30% sucrose solution, successively. After embedding in OCT media (Tissue-Tek, Sakura), frozen 12-μm sections were cut on a cryostat for histological analysis. Immunohistochemistry was performed using standard staining procedures with Neurogranin primary antibody (1:1000; Chemicon), followed by an Alexa-555-conjugated donkey anti-rabbit secondary antibody (Molecular Probes). For cell density analysis, the fixed brains were embedded in paraffin and 20-μm sections were cut on a microtome. To assay the number of cells in the IC, we quantified 3 cresyl violet stained sections

of the medial IC in each mouse using NIH ImageJ software, counting cells in an area of 1.65-mm^2 located centrally along the dorsal-ventral axis. Cells were chosen for quantification only if the nucleus was fully visible and in focus.

Analysis of whole brain and IC volume

As an initial comparison of anatomical phenotypes, we performed volumetric analyses of segmented brain and IC volumes. Using the propagating active contour filter in Amira software (TGS), whole brains were segmented semi-automatically, using manual editing to refine the contours from each individual *Fgf17*$^{+/-}$ *and Fgf17*$^{-/-}$ mouse. Whole brain templates were created using rigid, 12-parameter affine transformation for registration and averaging the groups of *Fgf17*$^{-/-}$ and *Fgf17*$^{+/-}$ mice separately. The registered mouse brain images were then normalized, adjusting the whole brain histograms to obtain equal mean and standard deviation (for later intensity-based analyses). ICs were extracted from the processed brain images using 3D IC masks created separately for *Fgf17*$^{-/-}$ and *Fgf17*$^{+/-}$ mice. The dorsal-caudal borders of the IC were easily identified by the adjacent cerebral spinal fluid (CSF) and cerebellum. The rostral border was identified by the decrease in Mn-enhancement in the IC compared to the superior colliculus, while the ventral borders were defined by the nucleus of the branchium of the IC and the CSF in the midbrain aqueduct. Using the resulting average masks, the IC was segmented, and the volume computed as the product of the voxel volume with the number of IC voxels, for each mouse. Whole brain and IC volumes were computed as the product of the voxel volume with the humber of brain and IC voxels, respectively. Differences in volume were analyzed statistically using Student's t-test (two-way), with significance set at $p<0.05$.

Deformation-based morphometry

Fgf17$^{+/-}$ and *Fgf17*$^{-/-}$ mice were analyzed for anatomical differences with unbiased deformation-based morphometry (DBM), using software obtained from the Mouse Imaging Centre (Toronto, Canada), which is based on image registration tools developed and distributed by the Montreal Neurological Institute (Collins et al., 1994). At completion of the registration process, local volume differences were identified computationally without prospective identification of anatomical structures. DBM methods for anatomical phenotyping in mice have been described previously (Kovacevic et al., 2005; Nieman et al., 2006, 2007; Lerch et al., 2008). The generation of a reference average image began by normalization of the orientation, location and intensity of all component images. Subsequently, an average space was defined that was unbiased to any particular image by averaging registration results of pair-wise image registrations (Woods et al., 1998). After generating an initial average in this orientation by taking the mean of image intensities at each voxel, each image was re-registered to the average iteratively to generate progressively refined averages. At each iteration, the registration was performed at a finer scale, until the final average with full-resolution (100-μm) was achieved. The final set of deformations from the *Fgf17*$^{+/-}$ and the *Fgf17*$^{-/-}$ groups to the average were then analyzed for significant anatomical differences. For volumetric differences, the local size changes encoded by the deformations were computed using the determinant of the Jacobian matrix, a multiplicative scale factor that represents voxel volume changes. A voxelwise Student's t-test of log-Jacobian values was used to identify regions of statistically significant change, correcting for multiple statistical comparisons using the false discovery rate (Benjamini and Hochberg, 1995).

Analysis of IC activity

The image analysis protocols for analyzing IC activity have been described in detail previously (Yu et al., 2008). Statistical analysis of MEMRI signals in the IC was performed voxel-wise with a two-tailed Student's t-test to compare the active IC volume between broadband sound stimulated and quiet control mice (Yu et al., 2005, 2008). To study the tonotopic organization within the IC, we analyzed the active IC volume after exposing mice to pure 16- and 40-kHz tones. In these experiments, maps of signal hyperintensity were created by setting a signal intensity (SI) threshold to be $SI_{Mean} + 1.5\ SI_{SD}$, where the mean (SI_{Mean}) and standard deviation (SI_{SD}) were measured from the histogram for each IC volume. The location of the active IC under pure tone conditions was located within the whole IC volume by measuring the distance between the centroids of each volume. Comparisons of the locations of the 16- and 40-kHz activity patterns in *Fgf17*$^{-/-}$ and *Fgf17*$^{+/-}$ mice were then made on the basis of their centroid locations (after averaging the left and right centroid locations for each mouse individually). For visualization of the variability between mice, the standard deviations of the centroid positions on each principal axis were used to define the radii of an ellipsoid, and the ellipsoids for the 16- and 40-kHz activity patterns were overlaid to show both the location and variability of the centroids for each activity pattern. Differences in centroid separation were analyzed statistically using Student's t-test (two-way), with significance set at $p<0.05$.

Region-of-interest (ROI) measurements were also made in the cochlear nucleus, as described previously (Yu et al., 2005), to determine whether there were any differences in the auditory input circuit, upstream of the IC, comparing *Fgf17*$^{-/-}$ and *Fgf17*$^{+/-}$ mice.

Results

ABR recordings show no peripheral hearing defects in Fgf17 mutant mice

ABR thresholds were measured in 4-week old WT ($N=4$), *Fgf17*$^{+/-}$ ($N=4$) and *Fgf17*$^{-/-}$ ($N=4$) littermates (Fig. 1). The 4-week age was chosen as the earliest developmental stage that consistent ABR recordings could be acquired with the existing experimental setup. There were no differences in the threshold responses after click (Fig. 1A) or pure tone (Fig. 1B) stimulation. We concluded that loss of *Fgf17* does not result in hearing impairment in these mice.

Analysis of anatomical brain phenotypes in Fgf17$^{-/-}$ *mice*

Analysis of whole brain and IC volumes was first performed using MEMRI images of small groups of P21 WT ($N=4$) and *Fgf17*$^{+/-}$ ($N=4$), confirming previous reports that there is no obvious phenotype in heterozygous *Fgf17* mutants (Xu et al., 2000). Volumetric and statistical analyses were then performed in larger groups of *Fgf17*$^{+/-}$ ($N=14$) and *Fgf17*$^{-/-}$ ($N=14$) mice, showing no differences in the whole brain volumes between WT, *Fgf17*$^{+/-}$ and *Fgf17*$^{-/-}$ mice (Fig. 2A), or in IC volumes between WT and *Fgf17*$^{+/-}$ mice, while the IC volume in *Fgf17*$^{-/-}$ mice was $17 \pm 5\%$ (mean ± standard deviation) smaller than in *Fgf17*$^{+/-}$ mice ($p=0.0001$; Fig. 2B), confirming the previous (qualitative) histological results (Xu et al., 2000). These results provide the first quantification of the anatomical IC phenotype of *Fgf17* knockout mice.

After MEMRI, brains were sectioned for histological analysis, staining for Neurogranin, a protein kinase C (PKC) substrate expressed by IC neurons (Huang et al., 1993; Neuner-Jehle et al., 1996). There was good qualitative agreement between *in vivo* MEMRI images (Figs. 2C,D) and Neurogranin staining (Figs. 2E,F). Note that Neurogranin is more highly expressed in the IC compared to adjacent brain regions, allowing identification of the IC nuclei in histological sections (Figs. 2E,F). Quantitative analysis of IC cell density revealed a 17% increase in *Fgf17*$^{-/-}$ ($N=3$) compared to *Fgf17*$^{+/-}$ ($N=3$) mice (Fig. 2G), closely matching the magnitude of the morphological decrease, and showing that the number of IC cells was not affected by loss of *Fgf17*.

To further explore the anatomical phenotypes in *Fgf17* mutant mice, automated and unbiased DBM analysis was performed to

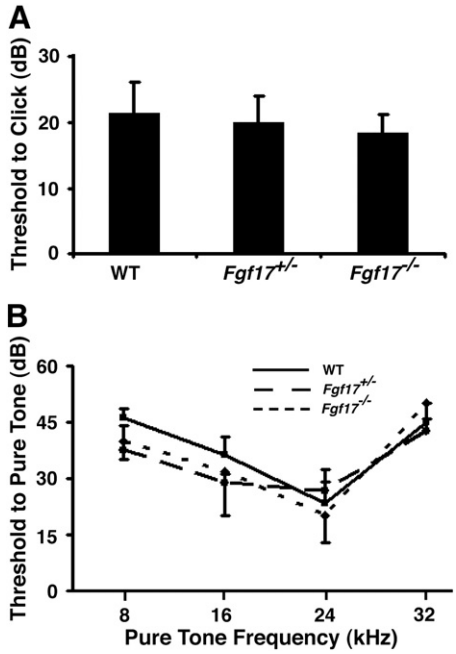

Fig. 1. ABR recordings detected no hearing deficits in *Fgf17* mutant mice. ABR threshold measurements after click stimulation were similar between $Fgf17^{+/+}$ wild type (WT), $Fgf17^{+/-}$, and $Fgf17^{-/-}$ mice (N = 4 for each genotype), with no significant difference between genotypes (A). During exposure to different pure tones, ABR threshold measurements were also similar among the three groups, with no statistically significant differences (B).

compare P21 $Fgf17^{-/-}$ (N = 10) and $Fgf17^{+/-}$ (N = 15) control mice (Fig. 3, false discovery rate, FDR = 0.05; Table 1). The resulting deformation maps showed small but statistically significant regional size differences between the two groups of mice. These included a reduced volume in the IC and anterior cerebellum in $Fgf17^{-/-}$ mice, and an increased volume in the fluid space above the IC, consistent with the IC deletion. In the forebrain, DBM analysis detected an expansion of the anterior-medial rhinal fissure, extending into the more lateral cortical regions suggesting possible alterations in the structure of the frontal cortex, previously undetected by histological analysis. Finally, the DBM maps showed a significant increase in the volume of a medial subregion of hypothalamus, and a decrease in the ventral-caudal olfactory bulb (OB), both previously undetected phenotypes in $Fgf17^{-/-}$ mutants.

MEMRI reveals a significant decrease in the active IC of $Fgf17^{-/-}$ mice

To assess the functional consequences resulting from loss of *Fgf17* during midbrain development, we analyzed regions of enhanced MEMRI signal in $Fgf17^{+/-}$ and $Fgf17^{-/-}$ mice after periods of defined sound stimulation. This approach was previously demonstrated to allow analysis of the functional core of the IC (Yu et al., 2005). For this analysis, we compared IC signal intensities between control mice kept in a quiet environment (Fig. 4A; N = 7 for each genotype) and mice stimulated with broadband sound, covering the entire audible frequency range for mice up to 59-kHz (Fig. 4B; N = 7 for each genotype). Consistent with the ABR data, analysis of signal intensities in the cochlear nucleus showed no differences between $Fgf17^{+/-}$ and $Fgf17^{-/-}$ mice (data not shown), indicating that any differences detected in the IC were not simply due to a global reduced activity in the auditory inputs of $Fgf17^{-/-}$ mice. Active IC regions for each genotype were characterized by 3D p-maps (Yu et al., 2008), consisting of voxels with significantly increased signal intensity compared to quiet controls ($p<0.05$, Fig. 4C). There was a 36% reduction in the average volume of the active IC, comparing $Fgf17^{-/-}$ (0.38-mm^3) and $Fgf17^{+/-}$ (0.60-mm^3) mice. When expressed as a ratio of active-to-total IC volume, the ratio in $Fgf17^{-/-}$ mice was still more than 20% lower than in $Fgf17^{+/-}$ littermates (Table 2). These results show that loss of *Fgf17* leads to a significant reduction in the volume of the IC region activated by auditory input, beyond that predicted by the morphological deletion.

MEMRI reveals a significantly altered IC tonotopic map in $Fgf17^{-/-}$ mice

To further examine the functional organization of the IC in *Fgf17* mutants, we compared tone-specific activity patterns in $Fgf17^{+/-}$ and $Fgf17^{-/-}$ mice. Frequency selectivity is a hallmark feature of the central auditory system, mainly attributed to the tonotopic projection of afferents into the IC and other auditory nuclei, which results in spatial patterning of tone-specific activity in each nucleus. In the normal IC, the tonotopic map is relatively simple, with lower frequencies activating more dorsal neurons, while higher frequencies activate more ventral neurons (Romand and Ehret, 1990). Longitudinal MEMRI experiments were performed to compare the positions

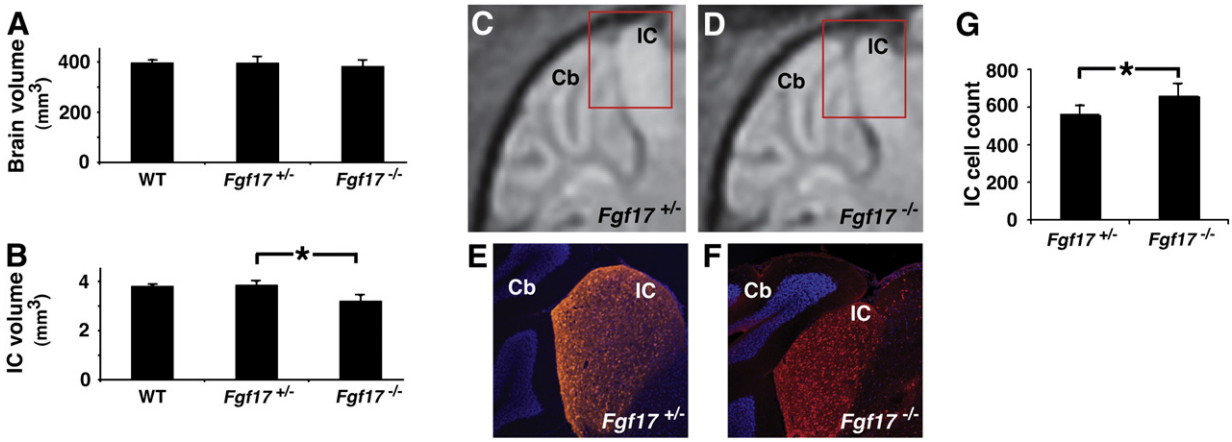

Fig. 2. MEMRI and histology confirmed the reduction of IC in $Fgf17^{-/-}$ mice. 3D MEMRI images of the brain and IC allowed quantitative volumetric analysis. Quantitative analysis showed no difference between the whole brain volumes of WT (N = 4), $Fgf17^{+/-}$ (N = 14) and $Fgf17^{-/-}$ mice (N = 14) (A), or between the IC volumes of WT and $Fgf17^{+/-}$ mice, while the IC volume in $Fgf17^{-/-}$ was significantly reduced compared to $Fgf17^{+/-}$ mice (B; *p = 0.0001). This reduction in IC size was also evident in sagittal MEMRI images (C,D) and matched histological (E,F), using Neurogranin (red) staining to identify the IC nuclei (A,B). Nuclear DAPI (blue) staining was used as a counterstain, highlighting the adjacent cerebellum (Cb). The red inset boxes (C,D) show the approximate position of the histological sections (E,F) relative to the MEMRI images. Quantitative analysis showed a significant increase in the number of cells per unit area in 3 slices of the central IC, comparing $Fgf17^{+/-}$ (N = 3) and $Fgf17^{-/-}$ (N = 3) mice (G; *p = 0.026).

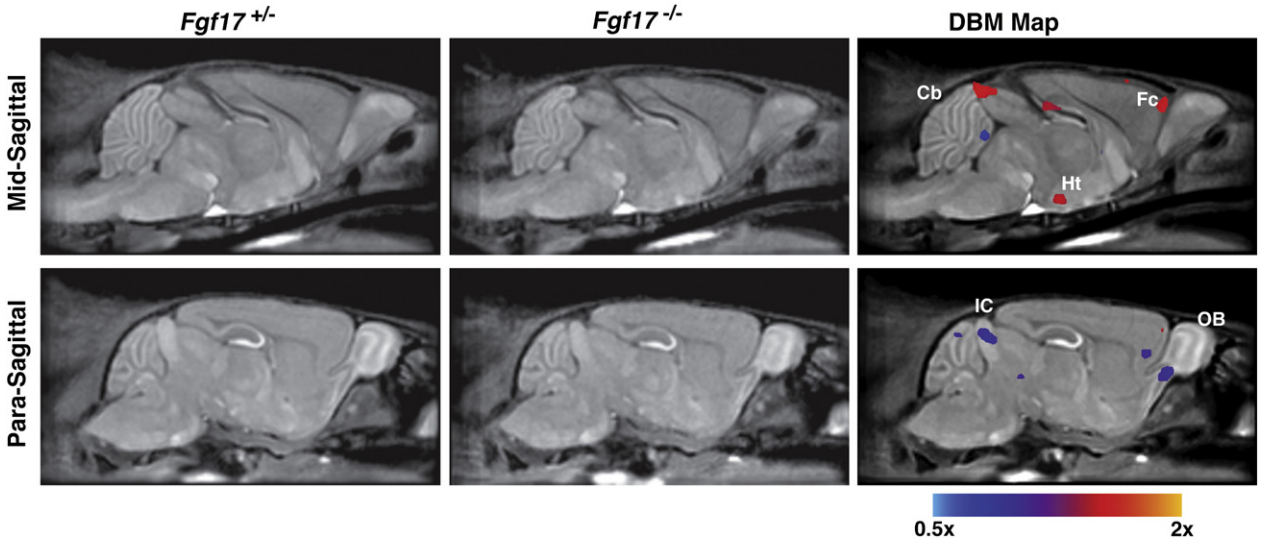

Fig. 3. DBM analysis revealed morphological differences in *Fgf17*$^{-/-}$ mice. Slices through 3D MRI datasets show the average *Fgf17*$^{+/-}$ and *Fgf17*$^{-/-}$ images, respectively, in the left and middle column. In the right column, statistically significant voxel size changes are highlighted (5% false discovery rate, FDR). The color scale indicates regions that were significantly larger (red/yellow; scale goes up to 2×) or smaller (blue; scale goes down to 0.5×) in the *Fgf17*$^{-/-}$ mice compared to the *Fgf17*$^{+/-}$ control littermates. Labels: cerebellum, Cb; frontal cortex, Fc; hypothalamus, Ht; inferior colliculus, IC; olfactory bulb, OB.

of 16- and 40-kHz IC activity patterns in both *Fgf17*$^{+/-}$ (N = 7) and *Fgf17*$^{-/-}$ (N = 10) mice. 40-kHz MEMRI data were first acquired in each mouse at P21. Mice were then kept in a quiet environment for two days to allow activity induced Mn accumulation to be cleared from the IC (Yu et al., 2005), after which 16-kHz MEMRI data were acquired in each mouse at P24. Tone-specific activity patterns were determined using thresholds based on the signal intensities in the MEMRI images (Yu et al., 2005).

In *Fgf17*$^{+/-}$ mice, 16- and 40-kHz activity patterns appeared normal (Yu et al., 2007), with well-separated domains aligned tonotopically along the dorsal-ventral axis of the IC (Fig. 5A). In contrast, the 16- and 40-kHz patterns were largely overlapping in *Fgf17*$^{-/-}$ mice, with only a small dorsal displacement of the 16-kHz region relative to 40-kHz region (Fig. 5B). Analysis of the distribution of tone-specific centroids (Figs. 5C,D) and statistical comparison of the spatial location of the centroids (Figs. 5E,F) both demonstrated and quantified the significantly reduced separation between the 16- and 40-kHz activity patterns in *Fgf17*$^{-/-}$ mice compared to *Fgf17*$^{+/-}$ controls. Specifically, the (16-40 kHz) centroid-centroid distance measured in *Fgf17*$^{-/-}$ mice was 49% smaller than *Fgf17*$^{+/-}$ controls. Interestingly, this centroid–centroid separation in *Fgf17*$^{+/-}$ mice (mean ± standard deviation = 351 ± 110 μm) was virtually identical to the distance measured in WT mice in a previous study (352 ± 27 μm; Yu *et al*., 2007), further confirming the lack of a detectable IC phenotype in *Fgf17*$^{+/-}$ heterozygous mutants. Taken together, these results indicate that in addition to the reduction in the size of the functional IC, there is also a significant alteration in the tonotopic organization of the IC in *Fgf17*$^{-/-}$ mutant mice.

Table 1
Summary of DBM results comparing *Fgf17*$^{-/-}$ and *Fgf17*$^{+/-}$ mice. There were significant volume decreases (−) in the inferior colliculus (IC), cerebellum (Cb) and olfactory bulb (OB), and significant volume increases (+) in the cerebral spinal fluid overlying the IC (IC-CSF), anterior-medial rhinal fissure (AM-RF), and the hypothalamus (Ht). DBM mapping was performed with a false discovery rate (FDR) of 0.05.

Mid-hindbrain			Forebrain		
IC	IC-CSF	Cb	AM-RF	Ht	OB
−	+	−	+	+	−

Finally, to determine whether the longitudinal imaging protocol might affect the second set of 16-kHz measurements, a separate group of *Fgf17*$^{-/-}$ mice (N = 6) was tested once only with 16-kHz stimulation at P21. There were no significant differences between these data and 16-kHz data from P24 *Fgf17*$^{-/-}$ mice after 40-kHz testing at P21 (Suppl. Fig. 1), showing that the longitudinal protocol used in these investigations was equivalent to testing individual groups of mice, between P21 and P24, at each frequency.

Discussion

This study provides the first *in vivo* quantitative analysis of morphological and functional defects in the brains of *Fgf17* knockout mice. In comparisons of 3D MEMRI images of *Fgf17*$^{+/-}$ and *Fgf17*$^{-/-}$ mutants, unbiased whole brain DBM analysis demonstrated significant morphological differences in the IC and cerebellum, regions previously reported to be altered based on histology (Xu et al., 2000). In addition, the olfactory bulbs in *Fgf17*$^{-/-}$ mice were found to be significantly smaller, while the fissure anterior to the medial frontal cortex, as well as more lateral frontal cortical regions were larger. This last result suggests a possible change in the anatomical structure of the frontal cortex in *Fgf17*$^{-/-}$ mice, an interesting finding given the altered gene expression in that region (Cholfin and Rubenstein, 2007), and the recent report of subtle cortical white matter abnormalities assessed by diffusion tensor imaging (Moldrich et al., 2010). In the IC there was good qualitative agreement between MEMRI and histology, while 3D MEMRI analysis was used to quantify the reduction in the *Fgf17*$^{-/-}$ IC volume. Interestingly, quantitative MEMRI activity mapping showed an even greater decrease in the active IC volume of *Fgf17*$^{-/-}$ mice after broadband sound stimulation. Moreover, the organization of IC neurons receiving auditory afferent projections is likely altered in *Fgf17*$^{-/-}$ mice, since the tone-specific (16- and 40-kHz) activity patterns were abnormal.

One question we aimed to address with our data was what is the relationship between the functional and anatomical phenotypes in *Fgf17*$^{-/-}$ mice. Some reduction in the volume of the active IC core might be expected in a smaller IC, without necessarily implying an altered organization of neurons and/or axonal projections in the IC of *Fgf17*$^{-/-}$ mice. Arguing against the possibility that the functional changes are simply byproducts of the altered morphology are the

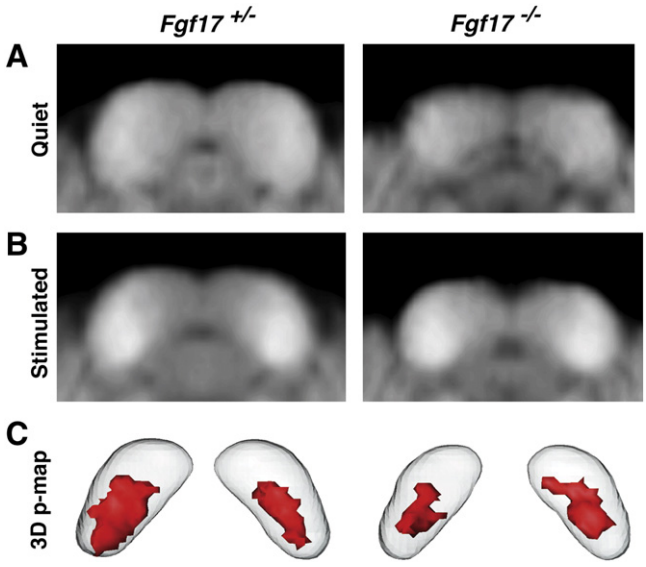

Fig. 4. MEMRI revealed a reduced functional IC in *Fgf17*$^{-/-}$ mice. Comparison of averaged coronal IC MEMRI images of mice maintained in a quiet environment (A) to mice exposed to broadband (1–59 kHz) sound stimuli (B) revealed MEMRI enhancement after stimulation in both *Fgf17*$^{+/-}$ (left) and *Fgf17*$^{-/-}$ (right) mice. Voxelwise statistical analysis identified the IC voxels with significant signal enhancement, displayed in 3D p-maps (C; red contours, $p \leq 0.05$), showing a reduction in the "active IC" of *Fgf17*$^{-/-}$ compared to *Fgf17*$^{+/-}$ mice.

relative magnitudes of the observed phenotypes. First, the decrease in active IC volume after broadband stimulation (36%) was more than twice the morphological decrease (17%). Furthermore, the distance between the centroids of the 16- and 40-kHz patterns was reduced by 49% in *Fgf17*$^{-/-}$ mice compared to *Fgf17*$^{+/-}$ mice, a reduction well beyond that necessary to accommodate either the IC or active-IC volume changes. It should be noted that the quantitative parameters derived from the statistical maps, and their relative magnitudes, should only be interpreted in comparisons between genotypes (*Fgf17*$^{-/-}$ vs. *Fgf17*$^{+/-}$), and not as absolute measures of brain activity, as measured, for example by electrophysiology. As with any statistical test, our choice of the $p<0.05$ detection threshold, although conventional, is somewhat arbitrary. Nevertheless, the statistical mapping results strongly suggest that the tonotopic organization of the IC is abnormal in *Fgf17*$^{-/-}$ mutants, leading us to speculate on the underlying cause of these changes. One possibility is that Fgf17 is involved in patterning the tonotopically ordered afferent innervations in the IC, which could be tested in future by performing axon-tracing studies, for example to determine whether defects exist in connectivity between IC and cochlea in *Fgf17*$^{-/-}$ mutants. Interestingly, there was no difference in the total number of IC cells in *Fgf17*$^{-/-}$ compared to *Fgf17*$^{+/-}$ mice, again suggesting that the functional differences are not a simple consequence of the morphological alterations.

It is also interesting to consider the current results in light of the behavioral abnormalities reported in *Fgf17*$^{-/-}$ mutant mice. The major behavioral phenotypes were decreased vocalizations of the mutant pups after isolation from their mothers, and decreased interaction time between adult *Fgf17*$^{-/-}$ males and wildtype females, and between *Fgf17*$^{-/-}$ male–female pairs after extended time in a novel environment, compared to wildtype pairs (Scearce-Levie et al., 2008). Although these behavioral phenotypes were previously attributed to changes in cortical gene expression, it is equally likely that they result from altered patterns of auditory activity implied by our data. Future investigation of auditory function is therefore important for understanding the *Fgf17*$^{-/-}$ behavioral phenotypes.

Table 2
Analysis of IC volumes and active-to-total IC volume ratios in *Fgf17*$^{-/-}$ and *Fgf17*$^{+/-}$ mice. Results are expressed as mean ± standard deviation for each entry.

Genotype	IC volume (mm^3)	Active to total IC volume ratio (%)
Fgf17$^{+/-}$	3.85 ± 0.16	15.87 ± 0.67
Fgf17$^{-/-}$	3.20 ± 0.24	12.09 ± 0.90

In the embryonic MHB, *Fgf8* expression is restricted to the anterior hindbrain, whereas *Fgf17* is more broadly expressed in the hindbrain as well as the posterior midbrain (anlage of the IC), and persists over a longer developmental window (Xu, et al., 2000; Liu et al., 2003). Based on mutant studies, Fgf17 is thought to play a secondary role to Fgf8 during embryogenesis, particularly during MHB development. Genetic studies in mutant zebrafish embryos (no isthmus, *noi* = *Pax2.1*; acerebellar, *ace* = *Fgf8*) detected no *Fgf17* expression in the MHB, indicating that Pax2.1 and Fgf8 are crucial upstream components in the pathway that activates Fgf17 (Lun and Brand, 1998; Reifers et al., 2000). Similarly, in *Fgf8* conditional mutant mice, *Fgf17* expression is lost after *Fgf8* is ablated (Chi et al., 2003). The separate roles of Fgf17 and two Fgf8 isoforms (Fgf8a and Fgf8b) have also been demonstrated in the mouse MHB. Fgf8b acts as a potent hindbrain organizer molecule, able to induce hindbrain genes and repress midbrain genes (Sato et al., 2001; Liu et al., 2003). In contrast, Fgf17, similar to Fgf8a, primarily induces midbrain structures (Liu et al., 2003). Since Fgf17 expression is lost in Fgf8 mutants, it cannot compensate for loss of Fgf8, likely accounting for part of the phenotypic difference between mice lacking *Fgf8* (Sun et al., 1999; Shamim et al., 1999; Chi et al., 2003) or *Fgf17* (Xu et al., 2000; Liu et al., 2003).

Our results show that loss of Fgf17 during embryonic brain development has a significant effect on postnatal brain function. Given the interactions between Fgf17 and Fgf8 during embryogenesis described above, it would be interesting in future to assess allelic series of *Fgf* mutants, comparing activity patterns in the brains of *Fgf17*, *Fgf8* and *Fgf8*/*17* double mutants, as well as conditional alleles of both genes. This would enable detailed analyses of the relationships between embryonic patterning defects due to misregulation of *Fgf* signaling and postnatal brain function. The abnormal tonotopic maps in the *Fgf17*$^{-/-}$ mice suggest that *Fgf* signaling is involved in the guidance of tonotopically organized afferents innervating the IC. However, it is still unclear whether Fgf17 directly regulates axonal targeting, or whether it regulates other guidance molecules indirectly. Thus, the molecular mechanisms of *Fgf* signaling in the formation of tonotopic maps remain to be uncovered. This study demonstrates the

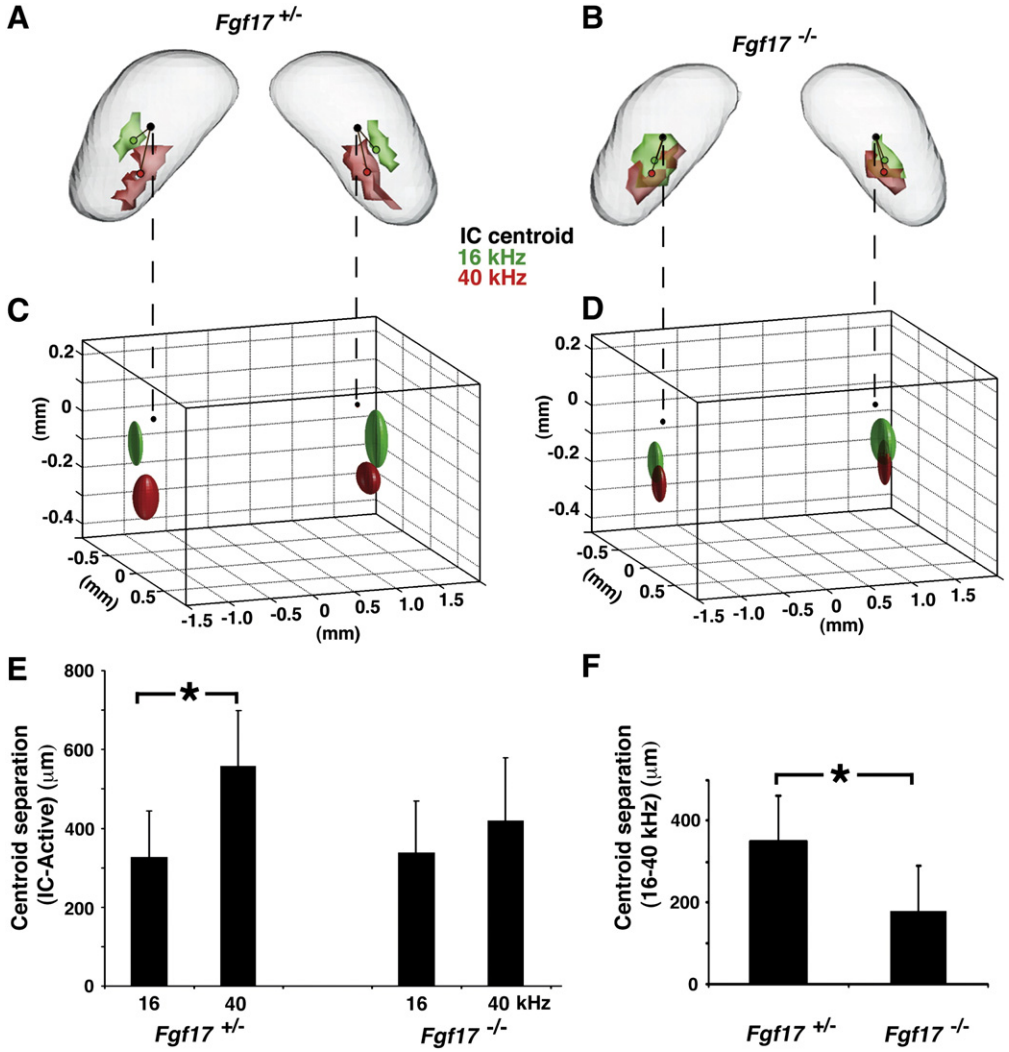

Fig. 5. MEMRI demonstrated an altered tonotopic map in *Fgf17*$^{-/-}$ IC. 16- (green) and 40-kHz (red) activity patterns and centroids (small green and red circles) were measured in the IC of *Fg17*$^{+/-}$ (A) and *Fg17*$^{-/-}$ (B) mice. The 16- and 40-kHz activity patterns were separated along the dorsal-ventral tonotopic axis in the IC of *Fgf17*$^{+/-}$ mice, but largely overlapped in *Fgf17*$^{-/-}$ mice. Likewise, ellipsoids representative of the population variability showed the normal separation in *Fgf17*$^{+/-}$ mice (C), but not *Fgf17*$^{-/-}$ mice (D). Quantitative analysis comparing the distance from each activity centroid to the IC centroid (small black circles) showed a significant difference in the two frequencies in *Fgf17*$^{+/-}$ mice, but not in *Fgf17*$^{-/-}$ mice (E; *p = 0.0057). There was also a 49% reduction in the separation between the 16- and 40-kHz centroids in *Fgf17*$^{-/-}$ mice compared to *Fgf17*$^{+/-}$ mice (F; *p = 0.0074).

importance of neuroimaging approaches like MEMRI and DBM for identifying and quantifying subtle changes in brain morphology, and for providing results that reveal functional abnormalities beyond the anatomical phenotypes. This study is also the first demonstration that MEMRI approaches can be applied to analyze functional phenotypes in the central auditory system of mutant mice. Importantly, MEMRI results can be used to guide future studies of altered circuitry and behavior in a variety of genetically engineered mice.

Supplementary materials related to this article can be found online at doi:10.1016/j.neuroimage.2011.02.068.

Acknowledgments

This research was supported in part by grants from the NIH (R01NS038461 and R01HD050767). We thank David Ornitz (Washington University) for providing the *Fgf17* mutant mice used in these studies, and Dan Sanes (NYU) for insightful discussions during the course of this work. We also thank Anand Mhatre (NYU School of Medicine) for advice on the ABR measurements, and Mark Henkelman, John Sled and Jason Lerch (Mouse Imaging Centre, Toronto Canada) for providing the software used for the DBM analysis.

References

Basson, M.A., Echevarria, D., Ahn, C.P., Sudarov, A., Joyner, A.L., Mason, I.J., Martinez, S., Martin, G.R., 2008. Specific regions within the embryonic midbrain and cerebellum require different levels of FGF signaling during development. Development 135, 889–898.

Benjamini, Y., Hochberg, Y., 1995. Controlling the false discovery rate—a practical and powerful approach to multiple testing. J. R. Stat. Soc. B Methodol. 57, 289–300.

Chi, C.L., Martinez, S., Wurst, W., Martin, G.R., 2003. The isthmic organizer signal FGF8 is required for cell survival in the prospective midbrain and cerebellum. Development 130, 2633–2644.

Cholfin, J.A., Rubenstein, J.L., 2007. Patterning of frontal cortex subdivisions by Fgf17. Proc. Natl. Acad. Sci. U. S. A. 104, 7652–7657.

Cholfin, J.A., Rubenstein, J.L., 2008. Frontal cortex subdivision patterning is coordinately regulated by Fgf8, Fgf17, and Emx2. J. Comp. Neurol. 509, 144–155.

Collins, D.L., Neelin, P., Peters, T.M., Evans, A.C., 1994. Automatic 3D intersubject registration of MR volumetric data in standardized Talairach space. J. Comput. Assist. Tomogr. 18, 192–205.

Crossley, P.H., Martinez, S., Martin, G.R., 1996. Midbrain development induced by FGF8 in the chick embryo. Nature 380, 66–68.

Fukuchi-Shimogori, T., Grove, E.A., 2001. Neocortex patterning by the secreted signaling molecule FGF8. Science 294, 1071–1074.

Fukuchi-Shimogori, T., Grove, E.A., 2003. Emx2 patterns the neocortex by regulating FGF positional signaling. Nat. Neurosci. 6, 825–831.
Garel, S., Huffman, K.J., Rubenstein, J.L., 2003. Molecular regionalization of the neocortex is disrupted in Fgf8 hypomorphic mutants. Development 130, 1903–1914.
Hoshikawa, M., Ohbayashi, N., Yonamine, A., Konishi, M., Ozaki, K., Fukui, S., Itoh, N., 1998. Structure and expression of a novel fibroblast growth factor, FGF-17, preferentially expressed in the embryonic brain. Biochem. Biophys. Res. Commun. 244, 187–191.
Huang, K.P., Huang, F.L., Chen, H.C., 1993. Characterization of a 7.5-kDa protein kinase C substrate (RC3 protein, neurogranin) from rat brain. Arch. Biochem. Biophys. 305, 570–580.
Kovacevic, N., Henderson, J.T., Chan, E., Lifshitz, N., Bishop, J., Evans, A.C., Henkelman, R.M., Chen, X.J., 2005. A three-dimensional MRI atlas of the mouse brain with estimates of the average and variability. Cereb. Cortex 15, 639–645.
Lee, S.M., Danielian, P.S., Fritzsch, B., McMahon, A.P., 1997. Evidence that FGF8 signaling from the midbrain–hindbrain junction regulates growth and polarity in the developing midbrain. Development 124, 959–969.
Lerch, J.P., Carroll, J.B., Spring, S., Bertram, L.N., Schwab, C., Hayden, M.R., Henkelman, R.M., 2008. Automated deformation analysis in the YAC128 Huntington disease mouse model. Neuroimage 39, 32–39.
Lin, Y.J., Koretsky, A.P., 1997. Manganese ion enhances T1-weighted MRI during brain activation: an approach to direct imaging of brain function. Magn. Reson. Med. 38, 378–388.
Liu, A., Li, J.Y., Bromleigh, C., Lao, Z., Niswander, L.A., Joyner, A.L., 2003. FGF17b and FGF18 have different midbrain regulatory properties from FGF8b or activated FGF receptors. Development 130, 6175–6185.
Lun, K., Brand, M., 1998. A series of no isthmus (noi) alleles of the zebrafish pax2.1 gene reveals multiple signaling events in development of the midbrain–hindbrain boundary. Development 125, 3049–3062.
Maruoka, Y., Ohbayashi, N., Hoshikawa, M., Itoh, N., Hogan, B.L., Furuta, Y., 1998. Comparison of the expression of three highly related genes, Fgf8, Fgf17 and Fgf18, in the mouse embryo. Mech. Dev. 74, 175–177.
Meyers, E.N., Lewandoski, M., Martin, G.R., 1998. An Fgf8 mutant allelic series generated by Cre- and Flp-mediated recombination. Nat. Genet. 18, 136–141.
Moldrich, R.X., Pannek, K., Hoch, R., Rubenstein, J.L., Kurniawan, N.D., Richards, L.J., 2010. Comparative mouse brain tractography of diffusion magnetic resonance imaging. Neuroimage 51, 1027–1036.
Neuner-Jehle, M., Denizot, J.P., Mallet, J., 1996. Neurogranin is locally concentrated in rat cortical and hippocampal neurons. Brain Res. 733, 149–154.
Nieman, B.J., Flenniken, A.M., Adamson, S.L., Henkelman, R.M., Sled, J.G., 2006. Anatomical phenotyping in the brain and skull of a mutant mouse by magnetic resonance imaging and computed tomography. Physiol. Genomics 24, 154–162.
Nieman, B.J., Lerch, J.P., Bock, N.A., Chen, X.J., Sled, J.G., Henkelman, R.M., 2007. Mouse behavioral mutants have neuroimaging abnormalities. Hum. Brain Mapp. 28, 567–575.
Reifers, F., Adams, J., Mason, I.J., Schulte-Merker, S., Brand, M., 2000. Overlapping and distinct functions provided by fgf17, a new zebrafish member of the Fgf8/17/18 subgroup of Fgfs. Mech. Dev. 99, 39–49.
Romand, R., Ehret, G., 1990. Development of tonotopy in the inferior colliculus. I. Electrophysiological mapping in house mice. Brain Res. Dev. Brain Res. 54, 221–234.
Sato, T., Araki, I., Nakamura, H., 2001. Inductive signal and tissue responsiveness defining the tectum and the cerebellum. Development 128, 2461–2469.
Scearce-Levie, K., Roberson, E.D., Gerstein, H., Cholfin, J.A., Mandiyan, V.S., Shah, N.M., Rubenstein, J.L., Mucke, L., 2008. Abnormal social behaviors in mice lacking Fgf17. Genes Brain Behav. 7, 344–354.
Shamim, H., Mahmood, R., Logan, C., Doherty, P., Lumsden, A., Mason, I., 1999. Sequential roles for Fgf4, En1 and Fgf8 in specification and regionalisation of the midbrain. Development 126, 945–959.
Shimamura, K., Rubenstein, J.L., 1997. Inductive interactions direct early regionalization of the mouse forebrain. Development 124, 2709–2718.
Storm, E.E., Garel, S., Borello, U., Hebert, J.M., Martinez, S., McConnell, S.K., Martin, G.R., Rubenstein, J.L., 2006. Dose-dependent functions of Fgf8 in regulating telencephalic patterning centers. Development 133, 1831–1844.
Sun, X., Meyers, E.N., Lewandoski, M., Martin, G.R., 1999. Targeted disruption of Fgf8 causes failure of cell migration in the gastrulating mouse embryo. Genes Dev. 13, 1834–1846.
Willott, J.F., 2006. Measurement of the auditory brainstem response (ABR) to study auditory sensitivity in mice. Curr. Protoc. Neurosci. (Ch 8, Unit 8.21B).
Woods, R.P., Grafton, S.T., Holmes, C.J., Cherry, S.R., Mazziotta, J.C., 1998. Automated image registration: I. General methods and intrasubject, intramodality validation. J. Comput. Assist. Tomogr. 22, 139–152.
Xu, J., Lawshe, A., MacArthur, C.A., Ornitz, D.M., 1999. Genomic structure, mapping, activity and expression of fibroblast growth factor 17. Mech. Dev. 83, 165–178.
Xu, J., Liu, Z., Ornitz, D.M., 2000. Temporal and spatial gradients of Fgf8 and Fgf17 regulate proliferation and differentiation of midline cerebellar structures. Development 127, 1833–1843.
Ye, W., Shimamura, K., Rubenstein, J.L., Hynes, M.A., Rosenthal, A., 1998. FGF and Shh signals control dopaminergic and serotonergic cell fate in the anterior neural plate. Cell 93, 755–766.
Yu, X., Wadghiri, Y.Z., Sanes, D.H., Turnbull, D.H., 2005. In vivo auditory brain mapping in mice with Mn-enhanced MRI. Nat. Neurosci. 8, 961–968.
Yu, X., Sanes, D.H., Aristizabal, O., Wadghiri, Y.Z., Turnbull, D.H., 2007. Large-scale reorganization of the tonotopic map in mouse auditory midbrain revealed by MRI. Proc. Natl. Acad. Sci. U. S. A. 104, 12193–12198.
Yu, X., Zou, J., Babb, J.S., Johnson, G., Sanes, D.H., Turnbull, D.H., 2008. Statistical mapping of sound-evoked activity in the mouse auditory midbrain using Mn-enhanced MRI. Neuroimage 39, 223–230.